Electrochimica Acta 355 (2020) 136773

Contents lists available at ScienceDirect

Electrochimica Acta

journal homepage: www.elsevier.com/locate/electacta

PEM fuel cells fed by hydrogen from ethanol dehydrogenation reaction: Unveiling the poisoning mechanisms of the by-products

Ana Laura G. Biancolli[1,*], Thiago Lopes[2,*], Valdecir A. Paganin, Edson A. Ticianelli

São Carlos Institute of Chemistry (IQSC), University of São Paulo, Ave Trabalhador Saocarlense 400, 13560-970 São Carlos, SP, Brazil

ARTICLE INFO

Article history:
Received 12 May 2020
Revised 12 July 2020
Accepted 13 July 2020
Available online 19 July 2020

Keywords:
Ethanol dehydrogenation
Contaminated hydrogen
Proton exchange fuel cell
Pt-based electrocatalysts
Hydrogen oxidation reaction

ABSTRACT

This work investigates the influence of hydrogen contaminated with the main by-products of the ethanol dehydrogenation reaction, i.e. ethyl acetate, acetaldehyde and unreacted ethanol, on the anode performance of a proton exchange membrane fuel cell employing different catalysts, aiming at understanding and minimizing the efficiency losses caused by these molecules. Pt-W/C and Pt-Sn/C catalysts were investigated, having Pt/C as reference, which were chosen due their ability to oxidize small organic molecules without breaking of C–C bonds and without producing strong poisoning intermediates (i.e. less prone to have its active sites blocked by side reactions). Results evidence that anode catalysts that presents lower activity for small organic molecules oxidation and/or weaker reactant adsorption, which is the case of Pt-Sn/C, are best suited for PEMFC systems directly fed by hydrogen from ethanol dehydrogenation reaction. It is also found that crossover of the considered by-products from the anode towards the cathode also has a major impact on fuel cell efficiency losses.

1. Introduction

Catalytic ethanol dehydrogenation has been proposed as a promising method to produce H_2 without CO and without significant CO_2 at mild reaction conditions and for onboard applications [1–3]. A specific work conducted by Sato et al. [2] had shown an ethanol dehydrogenation catalytic reactor coupled to a proton exchange fuel cell (PEMFC) to generate electricity for electric engines. A challenge with this system is that some ethanol dehydrogenation reaction by-products (mainly ethyl acetate, acetaldehyde and unreacted ethanol) contaminate the fuel cell causing not negligible power/efficiency losses. Nevertheless, an interesting fact is that these liquid by-product effluent from the reactor can also be used as fuel for an integrated internal combustion engine, or catalytically recycled to extract more hydrogen molecules. This increases the interest of the process, particularly when hybrid (electric/combustion) systems are considered.

Investigations on the effects of various contaminants on the performance of PEM fuel cell anodes are numerous, particularly when considering carbon monoxide and sulfur derivatives typically found in hydrogen produced by reforming of other fuels such as ethanol or natural gas [4]. In all cases, it has been demonstrated that the poisoning effect is caused by the strong adsorption of CO or S components on the catalyst active site (typically of Pt), which blocks the access of hydrogen to the metallic catalytic centers, reducing the extension of the hydrogen oxidation reaction (HOR) [5].

On the other hand, it has been observed that electrocatalysts formed by bimetallic Pt composites with Ru, W, Sn and Mo present enhanced tolerance to the presence of carbon monoxide, which is attributed to bifunctional and/or electronic effects [6–9]. The bifunctional effect is related to the fact that the second metal (Ru, W, Sn or Mo) acts to produce surface hydrated oxides at reaction overpotentials smaller than Pt, which are essential for the oxidation of CO adsorbed on Pt, thus liberating active sites for the hydrogen oxidation reaction. The electronic effect refers to the specific interaction of the atoms of the second metal with Pt, promoting an emptying of Pt 5d band. This phenomena decreases the electron back-donation of Pt to the adsorbed CO, which in turn reduces the bond strength and displaces the CO adsorption equilibrium freeing the Pt surface to the desired oxidation reaction [10,11].

These bimetallic electrocatalysts have been also successfully investigated for the direct oxidation of ethanol, where performances higher than pure Pt are evidenced. These studies have evidenced, in particular for Pt-Ru/C, that there is a dissociative oxidation of ethanol on the electrode that leads to the formation of -CHO and -COH adsorbed compounds, that also have poisoning action, similar

* Corresponding authors.
E-mail addresses: anabiancolli@hotmail.com (A.L.G. Biancolli), thiago_lopes@usp.br (T. Lopes).
[1] Present address: Nuclear and Energy Research Institute - IPEN - Ave Prof. Lineu Prestes 2242 - Butantã, São Paulo - SP 05508–000, Brazil.
[2] Present address: University of Sao Paulo, Escola Politecnica, Ave Prof Mello Moraes 2231, Sao Paulo-SP 05508030, Brazil.

https://doi.org/10.1016/j.electacta.2020.136773
0013-4686/

Table 1
EDX, XRD and TEM results for carbon-supported Pt and Pt-bimetallic catalysts.

Catalyst	EDX				XRD	TEM
	Pt (wt%)	C (wt%)	Sn or W (wt%)	Pt:Second metal (Atomic proportion)	Lattice Parameter	Mean particle size
Pt/C	20%	80%	–	–	0.399145 nm	2.9 nm
Pt-Sn/C	23%	69%	8%	2:1	0.399340 nm	4.3 nm
Pt-W/C	20%	75%	5%	4:1	0.399150 nm	5.2 nm

to that of CO. On the other hand, catalysts such as Pt-Sn/C and Pt-W/C are not so efficient for promoting the rupture of the C–C bond of ethanol, which minimizes the effects of the intermediates produced on Pt-Ru/C catalysts, but leads to lower energy utilization of ethanol due to the production of acetic acid as the main product, rather than CO_2 [12–15].

In a previous work [3], the influence of the main by-products of the ethanol dehydrogenation reaction (ethyl acetate, acetaldehyde and unreacted ethanol) on the performance of the PEM fuel cell containing Pt/C at cathode and anode was investigated. PEM single cell polarization measurements [3] showed that all by-products contaminate the anode catalyst, though the effect of ethanol is considerably higher when compared to acetaldehyde and ethyl acetate, at fixed concentrations of 1000 ppm. As a consequence, it has been found that unreacted ethanol plays the most important role in the anode poisoning, and thus in the decrease of the PEMFC performance.

To bring this practical interesting system closer to market application, fuel cell performances must be improved and the contamination effects have to be better understood and minimized. In this context, this work studied the effects of ethanol dehydrogenation reaction byproducts on a PEM single cell performance employing different anodic catalysts, aiming at understanding and minimizing the above mentioned PEMFC performance losses. The investigated catalysts were Pt-W/C and Pt-Sn/C, having Pt/C as reference. As mentioned above, these catalysts were chosen due to their ability to oxidize small organic molecules without breaking of C–C bonds and without producing strong poisoning intermediates.

2. Experimental

2.1. Catalysts

The synthesis of the Pt-Sn/C and Pt-W/C catalysts (see Table 1) were performed by the formic acid reduction method [16]. An appropriate mass of the carbon powder substrate (Vulcan XC-72C) was sonicated in 0.1 mol L^{-1} formic acid aqueous solution. This suspension was heated to 80 °C and the solution with the metal precursors was added in three portions. The suspension was then cooled to room temperature and then filtered. The resulting solid was finally oven dried at 80 °C for 1 h. The metal precursors used were $SnCl_4 \bullet 5H_2O$ for tin, $Na_2WO_4 \bullet 2H_2O$ for tungsten and $H_2PtCl_6 \bullet 6H_2O$ for Pt. The Pt/C catalyst 20 wt.% in metal was bought from E-tek®.

2.2. Characterization

Energy dispersive X-ray (EDX), transmission electron microscopy (TEM) and X-ray diffraction (XRD) techniques were used for the physical characterization of the catalyst materials. The EDX analyzes were carried out in an EDX LINK ANALYTICAL equipment (Isis System Series 200) with SiLi Pentafet detector, ATW II (Atmosphere Thin Window), with a resolution from 133 eV to 5.9 keV and 10 mm^2 area, coupled with a ZEISS LEO 440 Electronic Microscope (Cambridge, England). Co standard was used for calibration, electron beam of 20 kV, focal length of 25 mm, dead time of 30%, current of 2.82 A and I probe of 2.5 nA. The analyzed sample area was 640 × 640 μm.

X-ray diffraction signals were obtained in a Rigaku Rotaflex® equipment, Ru200B model. The measurements were conducted in a range of 2θ from 10 ° to 100 ° using Cu Kα radiation, with a scanning speed of 1 ° min^{-1}. TEM analyzes were performed at a JEOL equipment, EM2100 LaB6 model, 200KV. The samples were solubilized in isopropyl alcohol and deposited on a copper grid covered by a carbon film (EMS, 400 mesh).

High efficiency liquid chromatography (HPLC) was used to analyze the composition of the products that left the fuel cell (FC) anode (see Fig. 1) when it was fed by contaminated hydrogen. After condensation at −1.5 °C, the liquids were injected into a Shimadzu HPLC, Prominence Ultra-Fast Liquid Chromatograph, with refractive index (RID-10A) and UV–VIS (SPD-20A) detectors. The mobile phase was H_2SO_4 (3.33 mmol L^{-1}) and the chromato-

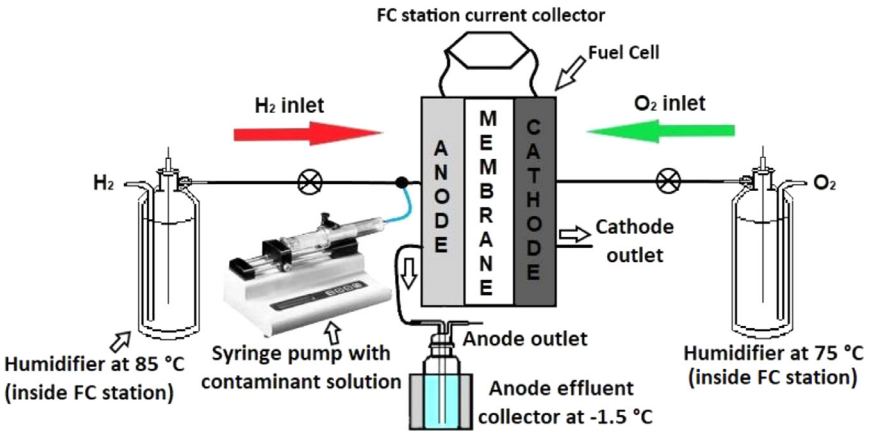

Fig. 1. Scheme of the system employed for the introduction of contaminants to the hydrogen stream supplied to the single fuel cell anode. The humidification chambers were located inside the fuel cell test station and at temperatures of 85 °C for the anode and 75 °C for the cathode. Each contaminant was introduced into the H_2 inlet pipe, which was thermally insulated. Post anode effluents were condensed at −1.5 °C in a collector for further HPLC analysis.

graphic column was Aminex HPX-87H. Analytical conditions: mobile phase flow = 0.6 mL min^{-1}, column temperature = 40 °C and scan time = 40 min. The chromatograms were corrected by the corresponding baselines for better interpretation of the results.

2.3. Contamination system

A syringe pump (KD Scientific Inc.) coupled to the hydrogen tubing PEMFC anode inlet (Fig. 1) was used to introduce the contaminants in order to simulate the gas composition in the outlet of the ethanol dehydrogenation reactor. This system was coupled to the FC anode, and used for controlled injections of solutions of each contaminant at a flow rate of the order of 10 mL h^{-1} in the hydrogen stream, so to reach concentrations at ppm levels. The contaminants under study were the main by-products of the ethanol dehydrogenation reaction: ethyl acetate, acetaldehyde and unreacted ethanol. The concentration of each contaminant solution was calculated to be 1000 ppm in the H_2 stream (flow rate = 100 mL min^{-1}). After circulating and eventually reacting in the anode, contaminants and their by-products were condensed in a recipient at −1.5 °C and immediately injected into the HPLC equipment. The effluents were collected during 10 min in each voltage (300 to 900 mV) to obtain optimal amounts of liquid and contaminant concentrations for appropriate HPLC analysis (this will be later seen in Fig. 5).

2.4. PEMFCs tests

The membrane and electrode assemblies (MEA) for the PEM single cell studies were prepared with standard gas diffusion electrodes (GDE) containing commercial Pt/C (E-tek), and homemade Pt-Sn/C or Pt-W/C catalysts for the anodes and Pt/C (E-tek) for the cathodes. All electrodes (4.62 cm^2 each) contained 0.4 mg cm^{-2} of Pt loading. The catalytic layer containing the electrocatalyst and 35.5% (w/w) of Nafion™ (Aldrich, 5wt%) was deposited on the GDEs by a well-established brushing procedure [17]. Finally, a pair of electrodes was hot pressed on both sides of a Nafion™ 115 membrane, following a very well-known procedure [17]. From here on, the fuel cell with Pt/C, Pt-W/C, and Pt-Sn/C in the anode will be named as Pt/Pt FC, Pt-W/Pt FC, and Pt-Sn/Pt FC, respectively.

The fuel cell was fed with pure H_2 or H_2 containing the by-products of the ethanol dehydrogenation (ethyl acetate, acetaldehyde or ethanol) at the anode and pure O_2 at the cathode, as described above (Fig. 1). The electrocatalysts already in the single cell electrodes were previously activated in pure H_2 flow at 70 °C for a period of 2 h and that temperature was maintained throughout all experiments. The polarization curves were obtained in galvanostatic mode in a test station provided by FCT - Fuel Cell Technologies, Inc.

Cyclic voltammetric (CV) curves of the anode were obtained by feeding it with argon while the cathode was fed with H_2, which simultaneously operated as a reference and auxiliary electrode. CVs of the cathode were obtained by using argon into the cathode while H_2 was used to feed the anode. The scan rate was 20 mV s^{-1} and both groups of experiments were performed at 70 °C.

Impedance Spectroscopy measurements were conducted with the PEMFCs fed with H_2 (contaminated and non-contaminated) at the anode and O_2 at the cathode, for all the studied electrocatalysts. The fuel cells were subjected to five currents set at: 73, 200, 300, 400 and 500 mA (current densities: 15.8, 43.3, 64.9, 86.6 and 108.2 mA cm^{-2}). The frequency ranged from 100 mHz to 100 kHz and the amplitudes of the AC (rms) signal were: 2.6 mA, 7.1 mA, 10.6 mA, 14.2 mA and 17.7 mA, respectively, for each set current (5% of the value of the currents used).

The experimental arrangement had the cathode as working electrode and the anode as reference and counter-electrode. Under the present experimental conditions, the proton transport resistance at the anodic catalyst layer can be considered negligible, as pure hydrogen and a 100% relative humidity condition was employed [18], and upon contamination, experiments evidence no changes in the high frequency resistance, nor the cathodic proton transport resistance. It is worth noting that the anode overpotential associated with the hydrogen oxidation reaction on experiments where the anode electrode is exposed to contamination by the by-products of the ethanol dehydrogenation reaction, falls below about 20 mV, as data presented in Section 3. The anode overpotentials were calculated by subtracting the oxygen reduction reaction overpotential (estimated from EIS) from the total cell overpotential, given that no differences were measured for the high frequency resistance, nor for the proton transport resistance at the cathodic catalyst layer. Detailed description of procedures involved in the EIS data processing using a single cell transmission line model is presented in the Section 3.2.

Considering the fast kinetics of the hydrogen reactions on platinum, and the high loading of catalyst on the anode catalyst layer, and the small overpotential estimated for the anode, this electrode was employed as counter and reference electrode in the EIS measurements carried out in the present work to estimate ohmic, ion transport and charge transfer (ORR) resistances. Furthermore, parallel reactions on the anode, upon cell contamination, would appear at lower frequencies on Nyquist or Bode plots as compared to the oxygen reduction reaction process, given the lower times constant of this process in comparison to the oxidation o small organic molecules [19]. This is apparently not seen on EIS data in the present work, which along with evidences of significant crossover of contaminants to the cathode electrode (see Figure S5) and the higher potential of this electrode supported an approach of considering changes on the “ORR arc” (i.e. Nyquist plot) a result of catalyst poisoning. The ORR charge transfer resistance extracted from EIS data fitting allowed for the estimation of the anode overpotential caused by electrode contamination with the ethanol dehydrogenation by-products:

$$\eta_{anode} = \eta_{cell} - \eta_{cathode(EIS)}$$

Where η_{cell} is measured from fuel cell polarization data with versus without exposure to contaminants. Similarly, $\eta_{cathode(EIS)}$ is estimated from the difference in the charge transfer resistance from EIS of fuel cells exposed versus not exposed to contaminants. Ohmic resistances and ionic transport resistances (at the membrane and catalyst layers) are not considered in the equation above, as both were observed not to be affected by the contaminants from fitted EIS data (e.g. see Fig. 3a).

3. Results and discussion

3.1. Electrocatalysts

EDX results for the synthesized Pt-Sn/C and Pt-W/C and the reference commercial catalyst Pt/C ETEK® are shown in Table 1. Results evidence that the Pt-Sn/C catalyst contains ca. 31 wt.% of metal supported on carbon with an atomic ratio of approximately Pt 2:1 Sn between the metals. For Pt-W/C catalyst, EDX analysis quantified ca. 25 wt.% of metal on carbon black with an atomic ratio of approximately Pt 4:1 W between the metals.

XRD diffractograms obtained for these catalysts are presented in Figure S1, where peaks characteristic to the face-centered cubic (fcc) lattice of Pt are seen, consistent with the responses of bimetallic platinum catalysts where this metal is the major component [6,9,20]. In the case of Pt-Sn/C, results show that the diffraction peaks are shifted to lower 2θ values when compared to Pt/C(Etek®). The lattice parameters of the Pt crystallites were calculated using the Bragg's formula and the results are included

in Table 1. The larger value of the lattice parameter given in Table 1 for Pt-Sn/C is consistent with the negative shift of 2θ (Fig. S1) and suggests an insertion of Sn atoms into the Pt crystal lattice, thus showing the formation of an alloy of Pt and Sn (Sn presents a larger atomic radius than Pt), which is not the case for Pt-W/C. For this latter catalyst, the result is consistent with the presence of pure Pt nanoparticles in contact with tungsten oxides (WO_x), as already observed in our group for a similar Pt-W/C composite [21].

Transmission electron microscopy images and corresponding particle size histograms for the above-mentioned catalysts (Pt/C, Pt-Sn/C and Pt-W/C) are presented in Figure S2. The histograms were obtained by measuring the size of at least 200 particles of each catalyst and applying a normal log function for fitting. Table 1 summarizes the values of the average particle sizes obtained from the histograms. Both, TEM images and histograms evidence narrow particle size distributions for the studied catalysts, with average values in the range of 3–5 nm, which are typically found for Pt-based catalysts prepared by the formic acid reduction method [22,23].

3.2. Electrochemical results

The influence of each ethanol dehydrogenation by-product on the performance of PEMFCs was studied with the contaminants separately injected in the H_2 stream under a fixed concentration (1000 ppm), for comparative purposes. Fig. 2 depicts polarization and total overpotential curves (i.e. loss of cell voltage caused by the contaminants) for the PEMFC with different anode catalysts. Comparing the effects of contaminants, these data evidence that unreacted ethanol causes the largest negative impact on PEMFCs performance, with the Pt/C anode-based cell presenting the largest effect (Fig. 2).

The polarization curves in Fig. 2b and 2c show that the PEMFC with the Pt-Sn/C anode exhibits somewhat higher performance compared to those with Pt/C or Pt-W/C, when the cell is fed with pure hydrogen. In addition, when the anode was exposed to the by-products of ethanol dehydrogenation, the overpotentials were noticeably smaller for the cell with the Pt-Sn/C anode (Fig. 2b), in comparison to those with Pt/C (Fig. 2a), especially for the cases of ethanol and ethyl acetate. On the other hand, Fig. 2c clearly shows that for the fuel cell employing Pt-W/C as anode, the overpotentials resulting from exposure to the contaminants are comparable and slightly smaller than that with Pt-Sn/C as anode. However, the performance of such cell, when fed with pure hydrogen, is significantly lower when compared to those with Pt/C or Pt-Sn/C anodes, resulting in the worst general performance among the PEMFCs studied here. It has been reported [24,25] that the presence of tin on Pt-based catalysts promotes the intrinsic catalytic activity of Pt towards the hydrogen oxidation reaction (HOR), when compared to pure Pt. On the other hand, worse performance for catalysts containing tungsten and platinum has been observed for the HOR, although they are more active than pure Pt when H_2 is contaminated with CO [21]. According to the characterization results discussed in the previous section, Pt-Sn/C has one Sn for every two Pt atoms, while Pt-W/C has one W for every four Pt. Also, both catalysts have larger particle sizes than Pt/C (4.3 nm for Pt-Sn/C and 5.2 nm for Pt-W/C). However, since the Pt loads are the same for all anodes (0.4 mgPt cm^{-2}), the effects observed on Fig. 2 for non-contaminated FCs may be related to the specific characteristics of each material, as for example formation of alloy between Pt and Sn, enhancing the activity, but this is not the case for Pt and W. In this last case, as previously mentioned, there are tungsten oxides that may be covering part of the active area of Pt, where the HOR effectively occurs, reducing the active area and so the overall activity. As it will be seen below, another point is that part of the tungsten migrates to the cathode, also causing overpotentials in the cathodic reaction, which contributes to the loss of overall fuel cell performance.

These results evidence that understanding the processes involved in the contamination of a PEMFC with ethanol dehydrogenation by-products requires analysis of the different phenomena that governs the fuel cell operation, in the absence and in the presence of the contaminants, which was carried out here through electrochemical impedance spectroscopy (EIS) and high-performance liquid chromatography (HPLC).

Results of electrochemical impedance spectroscopic measurements were employed to reach better understanding of the impacts of each contaminant on the PEMFC layers [26,27]. These data were processed using a transmission line model initially proposed by Eikerling and Kornyshev, as shown in Fig. S3 [28]. In this model, the AC impedance response of the cathode electrode can be described by a simple capacitance transmission-line model (Ccc, capacitance dependent on the potential of the catalytic layer) in parallel with resistances (Rcc, the resistance associate with the transport of protons in the catalytic layer, and Rct, the charge transfer resistance for the ORR), see Figure S3.

Fig. 3a shows Nyquist plots obtained at a current density of 64.9 mA cm^{-2} for the Pt-Sn/Pt FC fed with pure and contaminated H_2. In these diagrams, as described by Eikerling and Kornyshev [28], the proton transport effects within the cathodic catalytic layer can be analyzed in the region of high frequencies, where an approximately linear response with an angular coefficient of 45° is observed on the Nyquist plot, as shown in Fig. 3a. In this Figure, the arc represents the oxygen reduction reaction charge transfer resistance (series of resistors R_{tc}) connected in parallel with the capacitor with C_{cc} capacitance associated to the catalytic layer (see Fig. S3).

Fitting of the experimental data to the model using the equivalent circuit of Figure S3 allowed extracting the proton transport resistance in the cathodic catalytic layer, the charge transfer resistance of the oxygen reduction reaction, as well as the sum of the ohmic resistances associated with the transport of protons through the Nafion™ membrane and electrons through the different materials (e.g. diffusion layer and electric current collector plates). The fittings were performed using the ZView software from Scribner Associates. Fig. 3b illustrates an example of the fitting quality of the experimental data with the transmission line model, for the single cell with Pt/C catalyst in both electrodes. Fitting errors lower than 5% for the circuit components of the cell, and lower than 10% for the considered inductor, are observed for all the data in this work. Kramers-Kronig tests were also successfully carried out to proof the linearity and stability of the experiments [29] (Fig. S4).

EIS data for the Pt-W/Pt FC and Pt-Sn/Pt FC follows the same trend illustrated in Fig. 3a and evidence that both the high frequency resistance and the proton transport resistance are not affected by contaminants, contributing less than 1 mV to the total overpotential (within the experimental error), while the oxygen reduction reaction might be affected because of a crossover of contaminants from the anode to the cathode, as evidenced by cyclic voltammograms of the cathodic catalyst after the poisoning experiments (see Figure S5) and by EIS data, as follows. This crossover effect leads to PEMFC performance losses due to reaction overpotentials (η_C^c) arising in the cathode, which can be estimated by EIS fittings. Furthermore, with the use of the total fuel cell overpotential (η_T^c) (as shown in Fig 2), the contribution of the anode (η_A^c) can be estimated as ($\eta_A^c = \eta_T^c - \eta_C^c$). All these results are shown in Fig. 4.

Plots in Fig. 4 show that, except for ethyl acetate, the overpotentials ($\eta_A^c, \eta_T^c, \eta_C^c$) for the other contaminants are lower when the PEMFC anodes are Pt-Sn/C or Pt-W/C, in comparison to Pt/C, in agreement with what has been observed from Fig 2, with ethanol resulting the highest overpotentials. Very importantly, the pres-

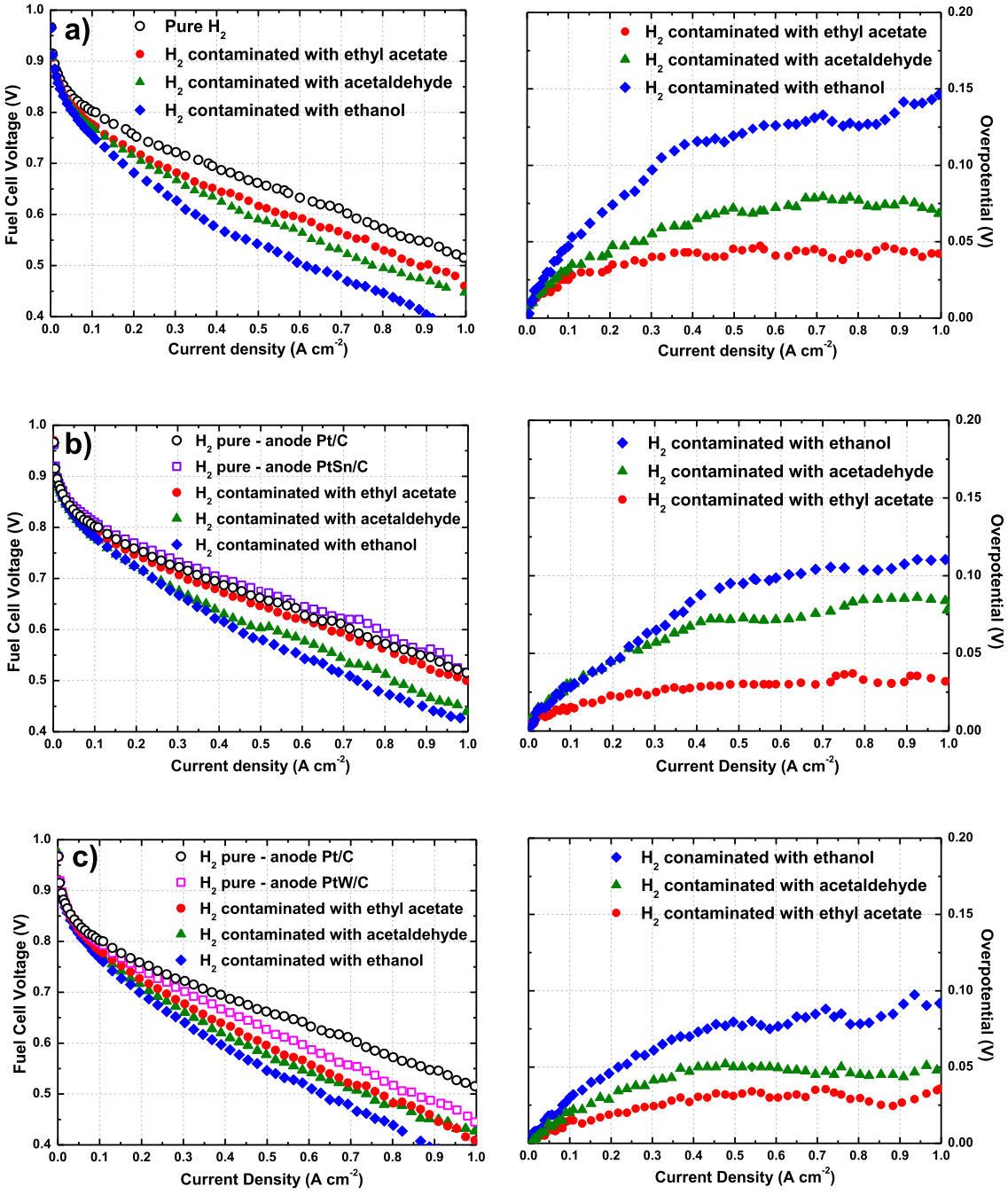

Fig. 2. **a)** Steady state polarization curves of Pt/Pt FC (on the left side) and the corresponding total overpotential curves (on the right side); **b)** same for PtSn/Pt FC (Pt-Sn/C on the anode); **c)** same for PtW/Pt FC (Pt-W/C on the anode). Fuel cell fed with H_2 contaminated by main by-products of ethanol dehydrogenation reaction compared to pure H_2-fed anode. Anode: Pure H_2 or contaminated H_2 (flow rate = 100 mL min^{-1}); Cathode: pure oxygen (flow rate = 150 mL min^{-1}). T_{cell} = 70 °C, Pt loads: 0.40 ± 0.01 mg_{Pt} cm^{-2}.

ence of cathodic overpotentials introduced by the contaminants is clearly evidenced, confirming their influence on the kinetics of the oxygen reduction reaction.

The negative anode overpotential seen for the Pt-W/C based PEMFC at low current densities is consistent with a crossover of tungsten from the anode to the cathode along the experiments leading to more Pt active sites available to catalyze the hydrogen oxidation reaction. This is corroborated by the cyclic voltammetry analysis shown in Figure S5c, where the peaks in the hydrogen region of platinum of the CV of the anode clearly start to appear after the PEMFC contamination experiments. In agreement with this, the cyclic voltammogram of the cathodic electrode on Pt-W/C based cells indicated the presence of tungsten in this electrode (Figure S6), confirming a crossover of this metal from the anode to the cathode. This is corroborated by the higher values of the charge transfer resistance obtained from EIS fitting data for these cells (note that the cathode catalyst employed, Pt/C, is the same in all cells). Comparing EIS data for Pt-W/Pt FC and Pt/Pt FC at 0.108 A cm^{-2}, it is first noticed a suitable reproducibility of MEA preparation by negligible changes (< 1 mΩ cm^{-2}) on the high frequency resistance (HFR) and the proton transport resistance at the cathodic catalyst layer. However, even though made out of the same material, the higher ORR charge transfer resistance measured for the Pt-W/Pt FC accounts for 60% of the total difference in per-

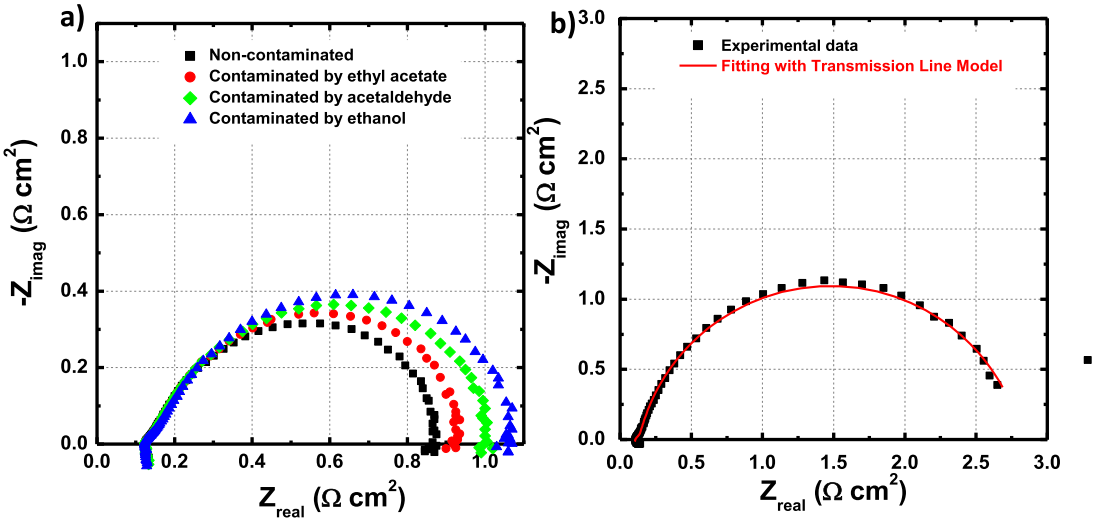

Fig. 3. Nyquist plots of the complex-plane impedance of the electrode membrane assembly having **a)** Pt-Sn on the anode and Pt/C on the cathode. DC current density of 64.9 mA cm^{-2}. Fuel cell fed by pure H_2 (black squares) or contaminated H_2 (ethanol = blue triangles, ethyl acetate = red circles and acetaldehyde = green rhombus) and O_2. AC was 5% of the DC value, with AC variation frequencies from 100 kHz to 0.1 Hz, T_{cell} = 70 °C and under flow rate of 100 mL min^{-1} for H_2 and 150 mL min^{-1} for O_2. **b)** Pt/C catalyst in both electrodes. DC current density of 15.8 mA cm^{-2}. Fuel cell fed by pure H_2 and O_2. Black squares represent the experimental data and red line the fitting using a transmission-line model.

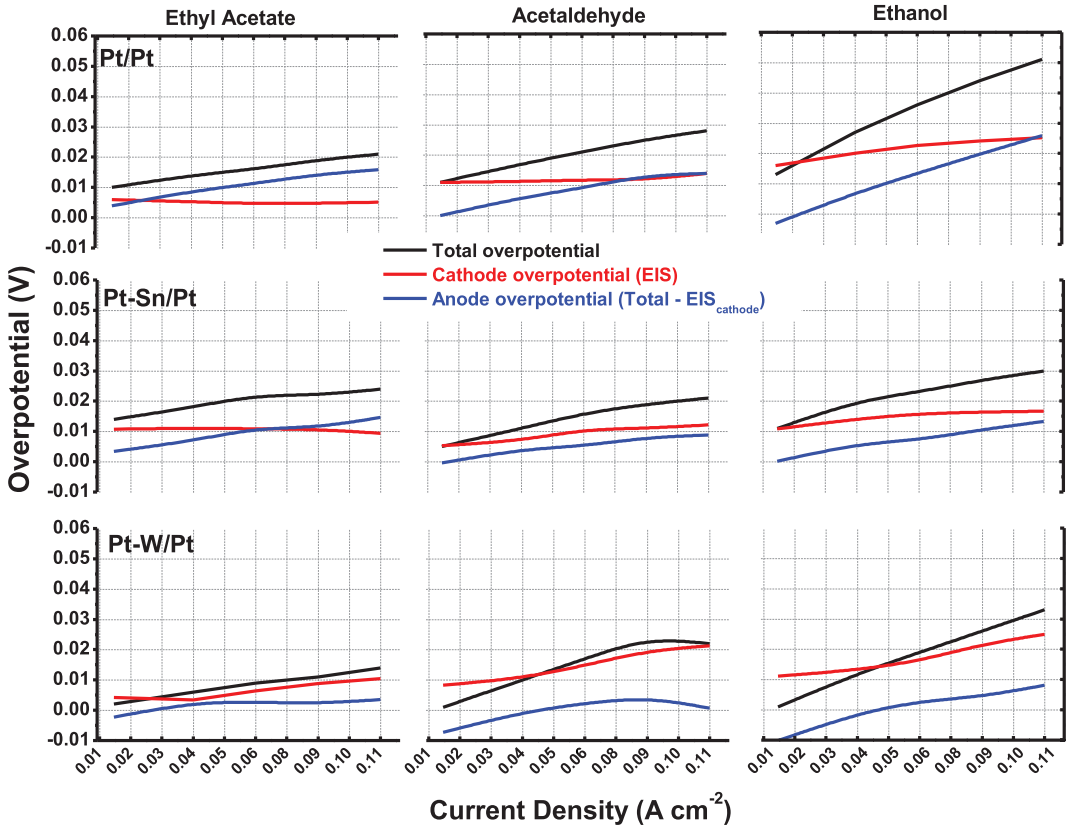

Fig. 4. Fuel cell overpotential break down: total overpotential (η_T^c), anode overpotential (η_A^c) and cathode overpotential (η_C^c) (difference between uncontaminated and contaminated fuel cell overpotentials) as a function of current densities (15.8; 43.3; 64.9; 86.6 and 108.2 mA cm^{-2}).

formance between the cells, compared to Pt/Pt FC. It is interesting noting that even though a crossover of tungsten is noticed (Figure S6), no changes are measured for the high frequency resistance of Pt-W/C anode based cells (nor others), suggesting that the migration of tungsten is not associated with cations. It is worth noting that even at a small contamination of Nafion^{TM} with cations, an increase on the high frequency resistance of a MEA is clearly noticed as the current density increases, due to the accumulation of non-reacting cations at the cathodic side of the membrane by migration, hindering the transport of protons [30–32].

Another interesting fact observed in Fig. 4 is that the cathodic overpotentials are generally higher than the anodic ones, within the current density range analyzed. However, the anode overpotentials induced by the contaminants, present a tendency to in-

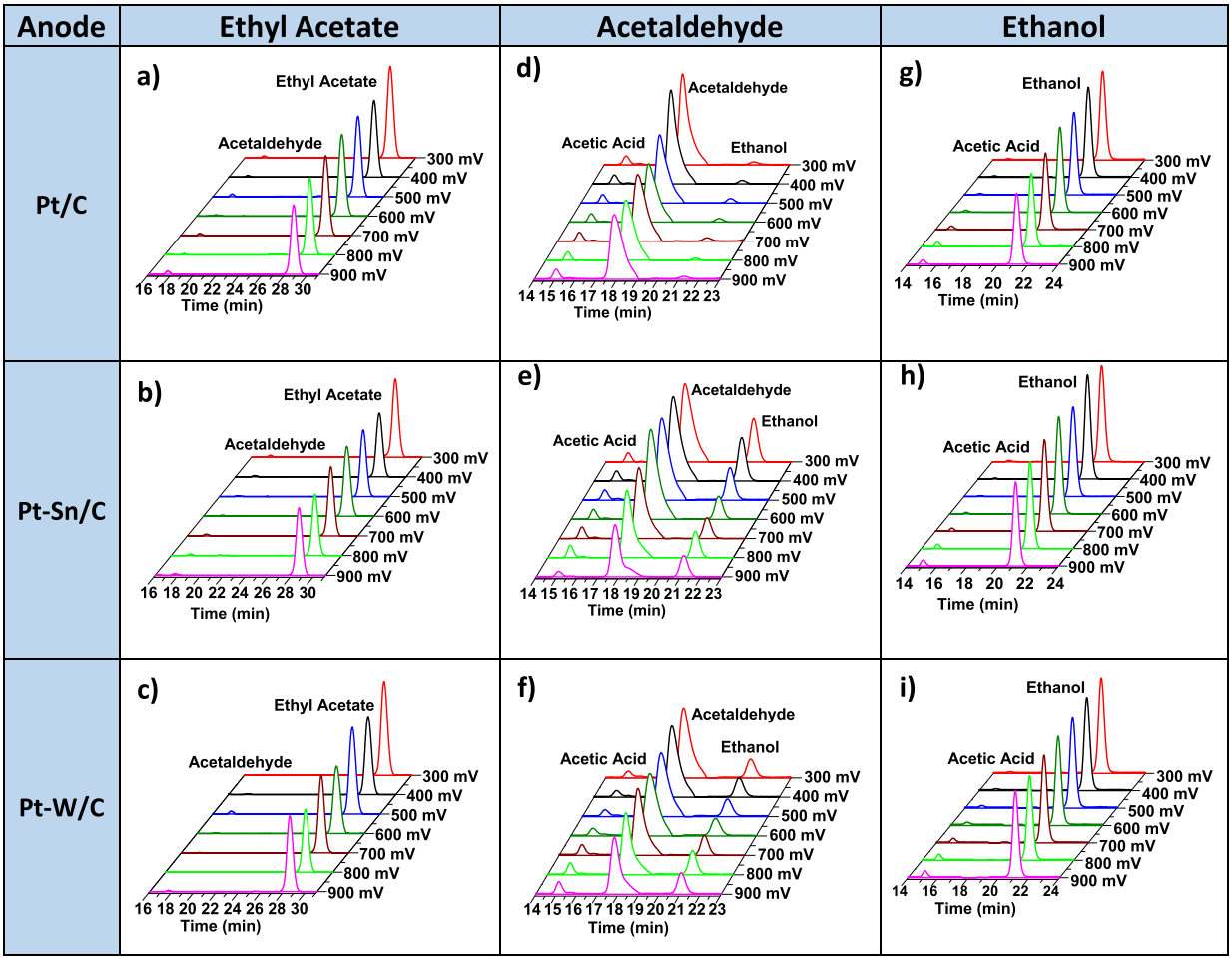

Fig. 5. High performance liquid chromatograms of PEMFC anode effluents when exposed to 1000 ppm of ethyl acetate, acetaldehyde and ethanol at various fuel cell voltages and anodic electrocatalysts under study. Detectors: refractive index (RID-10A) and UV–vis (210 nm). Observed peaks: acetic acid in 15 min; acetaldehyde in 18 min; ethanol in 21 min; ethyl acetate in 29 min.

crease with the increase of current density, becoming higher than for the cathode at higher current density values, especially for the Pt/Pt FC. In fact, in Fig. 4 it is seen that the cathodic overpotential tends to flatten out as current density increases, except for Pt-W/Pt FC in which case there is a raise of the overpotential due to tungsten crossover. Both phenomena, the anode overpotential augments and the cathode overpotential flatting out, can be associated to the crossover of the contaminant because when the overpotential increases more contaminant is oxidized in the anode, so becoming less available to cross membrane to reach the cathode. This is further discussed in the next section.

Finally, and as mentioned before, it is noted from data presented in Fig. 4 that ethanol is the most significant contaminant, while ethyl acetate is apparently the least. This might be associated to its lower solubility in water [33,34] making it less susceptible to cross the membrane to reach the cathode and to impact the oxygen reduction reaction kinetics.

3.3. High performance liquid chromatography (HPLC) results

High performance liquid chromatography (HPLC) analyses of the anode effluents collected by condensation along the experiments were conducted at different cell potentials so to search for products eventually formed by reactions of the contaminants within the electrodes. Fig. 5 shows these chromatograms for the different contaminants and anode materials, plotted for the different cell voltages. Fig. 5a-c shows that when the contaminant is ethyl acetate, the detected product, besides its own, includes a very small quantity of acetaldehyde, as seen using UV–vis detector. Using refractive index detector, it was also possible to detect formation of some ethanol by the decomposition reaction [35] (Reaction (1)), but the quantity is so small that no ethanol signal appeared in Fig. 5a-c.

$$CH_3COOC_2H_5 + H_2 \overset{Pt}{\rightleftharpoons} CH_3CH_2OH + CH_3CHO \quad \text{(Reaction 1)}$$

When acetaldehyde contamination is considered (Figs 5d-f), formations of ethanol and acetic acid are observed in all cases, though in different proportions depending on the composition of the anodic catalyst. Possible processes leading to the formation of ethanol and acetic acid from acetaldehyde are [36]:

$$CH_3CHO + H_2 \rightleftharpoons CH_3CH_2OH \quad \text{(Reaction 2)}$$

$$CH_3CHO + Pt \rightleftharpoons Pt\text{-}(CO\text{–}CH_3)_{ads} + H^+ + e^- \quad \text{(Reaction 3a)}$$

$$Pt\text{-}(CO\text{–}CH_3)_{ads} + M(OH)_{ads} \rightarrow Pt + M + CH_3COOH \quad \text{(Reaction 3b)}$$

In this way, ethanol is suggested to be formed through a chemical reduction of acetaldehyde with molecular hydrogen

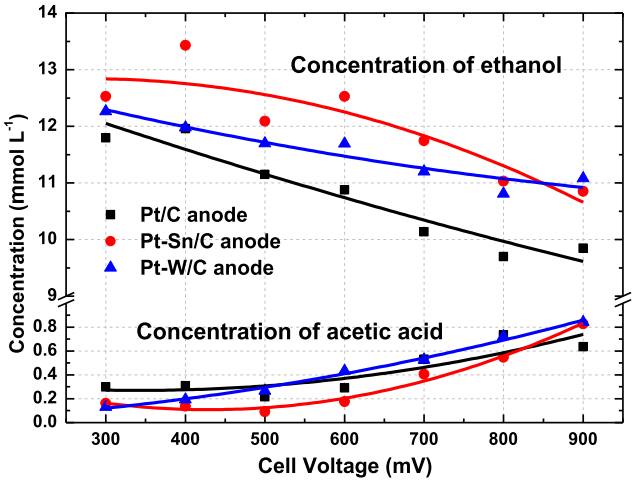

Fig. 6. Estimated concentration of ethanol and its conversion product (acetic acid) at the anode outlet of a PEMFC during exposure of the anode electrode to ethanol contaminant (main poison from dehydrogenation reaction), as a function of cell voltage. Anode: contaminated H_2 (flow rate = 100 mL min^{-1}); Cathode: pure oxygen (flow rate = 150 mL min^{-1}). T_{cell} = 70 °C, Pt loads: 0.40 ± 0.01 mg_{Pt} cm^{-2}. Effluents collected in each voltage after 10 min.

(Reaction (2)), while acetic acid may be formed by the oxidation of acetaldehyde in the anodic catalyst, that produces an adsorbed intermediate (Reaction (3a)), which next reacts with a metallic hydrous oxide (Reaction (3b)). It is interesting noting that higher amounts of ethanol tend to be observed for systems (fuel cells) containing bimetallic electrocatalysts. At low temperatures (<150 °C) the hydrogenation of acetaldehyde (Reaction (2)) is the main reaction that takes place [37], and it seems likely that the presence of the second metal increases its selectivity.

When hydrogen was contaminated with ethanol, Fig. 5g-i, the formation of acetic acid was observed in all cases, possibly by the following reactions:

$$CH_3CH_2OH + H_2O \rightarrow CH_3COOH + 4H^+ + 4e^- \quad \text{(Reaction 4)}$$

or

$$CH_3CH_2OH + O_2 \rightarrow CH_3COOH + H_2O \quad \text{(Reaction 5)}$$

or

$$Pt + CH_3CH_2OH \rightarrow Pt\text{-}(CHOH\text{-}CH_3)_{ads} \text{ or } Pt\text{-}(OCH_2\text{-}CH_3)_{ads} + e^- + H^+ \quad \text{(Reaction 6a)}$$

$$Pt\text{-}(CHOH\text{-}CH_3)_{ads} \text{ or } Pt\text{-}(OCH_2\text{-}CH_3)_{ads} \rightarrow Pt + CHO\text{-}CH_3 + e^- + H^+ \quad \text{(Reaction 6b)}$$

these two latter, being followed by Reactions (3a) and (3b).

It is interesting to note that acetic acid is formed at higher proportions at higher cell voltages or lower current densities. Since the mass flux of O_2 in the cathode is in excess at low current densities, higher amount of oxygen is unutilized implying that more oxygen is available to diffuse across the membrane from the cathode to the anode. This molecular oxygen could potentially promote the oxidation of ethanol to acetic acid, as evidenced by data in Fig. 6, where a decrease of ethanol concentrations is also clearly detected at higher cell voltages. This fact might also be promoted by the greater solubility of oxygen in the water/ethanol mixture, compared to pure water [38]. Reactions 6a and 6b followed by Reactions (3a) and (3b) are the very well-known electro-oxidation reactions of ethanol forming acetic acid [39–41]. Sn is able to adsorb water dissociatively to form adsorbed OH species and allows the formation of CH_3COOH at lower overpotentials and with relatively fast kinetics.

Data in Fig. 6 compares the relative concentration of compounds at the anode outlet of a PEMFC upon contamination with ethanol, obtained using the area of peaks in Fig. 5 and a calibration curve. Only data relative to the concentration of the ethanol contaminant is considered here, as it is the main contaminant of the system. Besides, similar data analyses conducted for the ethyl acetate and acetaldehyde contaminations are scattered and less prone for drawing conclusions; this experimental difficulty is most probably consequence of the lower water solubility of ethyl acetate [33] and the lower boiling point of acetaldehyde.

Fig. 6 shows that contamination of the anode with ethanol resulted in higher concentration of this molecule in the outlet when using the Pt-Sn/C anode. This suggests that in this catalyst, a reduced concentration of ethanol is converted into products, and this is consistent with the smaller concentration of oxidation products (acetic acid) seen for this electrode material. Since less catalyst active sites are involved in the ethanol oxidation process, more free sites are available for the HOR so that smaller anode overpotentials should be seen for the cell with Pt-Sn/C anode, as confirmed by results in Fig. 4. Data in Fig. 6 also evidences that, in general, catalysts that "consume" less contaminant tend to promote higher power densities on the fuel cell device (Figs. 2), being Pt/C the worst and Pt-Sn/C the best, in the present work. This trend interestingly corroborates with data in Fig. 4, where, generally, Pt/C presents higher and Pt-Sn/C lower anode electrode overpotentials, compatible with a higher oxidation rate of contaminants on Pt compared to Pt-Sn/C (i.e. more positive electrode potential leads to higher reaction rates). Furthermore, Silva et al. [42] concluded that non-alloyed Pt catalysts favor the C–C bond breaking but at low reaction kinetics; this leads to the conclusion that the ethanol molecule probably remains adsorbed in Pt much longer in Pt/C as compared to Pt-Sn/C.

4. Conclusions

The thorough analysis carried out here points to a general conclusion that anode catalysts that presents a lower activity for small organic molecules oxidation and/or promote a weaker adsorption, and/or presents a lower electrode overpotential (higher exchange current density for the hydrogen oxidation reaction) would seem to be best suited for the present interesting approach involving the on line coupling of the ethanol dehydrogenation reaction to a fuel cell towards practical applications.

Although this study shows that the use of the Pt-Sn/C catalyst can potentially increase the power density of fuel cells fed by hydrogen from the ethanol dehydrogenation reaction without the addition of new apparatus, it also points out that crossover of the by-products of this reaction towards the cathode also has a major impact on FC efficiency loss. This happens especially in the case of ethanol and acetaldehyde, which are 100% water-soluble molecules and probably can more easily cross the Nafion™ membrane. In this context, further studies of the impact of these by-products on the fuel cells cathodes seem necessary for a more complete understanding of the involved effects.

Declaration of Competing Interest

The authors declare that they have no known competing financial interests or personal relationships that could have appeared to influence the work reported in this paper.

CRediT authorship contribution statement

Ana Laura G. Biancolli: Visualization, Data curation, Conceptualization, Writing - review & editing. **Thiago Lopes:** Conceptualization, Formal analysis, Writing - review & editing. **Valdecir A. Paganin:** Visualization, Data curation. **Edson A. Ticianelli:** Supervision, Project administration, Conceptualization, Writing - review & editing.

Acknowledgments

Authors thank the financial support from The São Paulo Research Foundation (FAPESP) processes: 2013/16930–7, 2014/22130–6, 2015/09210–3, 2016/13277–9 and 2017/15304–6.

Supplementary materials

Supplementary material associated with this article can be found, in the online version, at doi:10.1016/j.electacta.2020.136773.

References

[1] D. Gao, Y. Feng, H. Yin, A. Wang, T. Jiang, Coupling reaction between ethanol dehydrogenation and maleic anhydride hydrogenation catalyzed by Cu/Al2O3, Cu/ZrO2, and Cu/ZnO catalysts, Chem. Eng. J. 233 (2013) 349–359, doi:10.1016/j.cej.2013.08.058.

[2] A.G. Sato, G.C.D. Silva, V.A. Paganin, A.L.G. Biancolli, E.A. Ticianelli, New, efficient and viable system for ethanol fuel utilization on combined electric/internal combustion engine vehicles, J. Power Sources 294 (2015) 569–573, doi:10.1016/j.jpowsour.2015.06.086.

[3] A.G. Sato, A.L.G. Biancolli, V.A. Paganin, G.C. Da Silva, G. Cruz, A.M. Dos Santos, E.A. Ticianelli, Potential applications of the hydrogen and the high energy biofuel blend produced by ethanol dehydrogenation on a Cu/ZrO2catalyst, Int. J. Hydrogen Energy 40 (2015) 14716–14722, doi:10.1016/j.ijhydene.2015.05.071.

[4] X. Cheng, Z. Shi, N. Glass, L. Zhang, J. Zhang, D. Song, Z.-S. Liu, H. Wang, J. Shen, A review of PEM hydrogen fuel cell contamination: impacts, mechanisms, and mitigation, J. Power Sources 165 (2007) 739–756, doi:10.1016/j.jpowsour.2006.12.012.

[5] T. Lopes, V.A. Paganin, E.R. Gonzalez, The effects of hydrogen sulfide on the polymer electrolyte membrane fuel cell anode catalyst: H2S-Pt/C interaction products, J. Power Sources 196 (2011) 6256–6263, doi:10.1016/j.jpowsour.2011.04.017.

[6] P.P. Lopes, K.S. Freitas, E.A. Ticianelli, CO tolerance of PEMFC anodes: mechanisms and electrode designs, Electrocatalysis 1 (2010) 200–212, doi:10.1007/s12678-010-0025-y.

[7] T.C.M. Nepel, P.P. Lopes, V.A. Paganin, E.A. Ticianelli, CO tolerance of proton exchange membrane fuel cells with Pt/C and PtMo/C anodes operating at high temperatures: a mass spectrometry investigation, Electrochim. Acta 88 (2013) 217–224, doi:10.1016/j.electacta.2012.10.039.

[8] F.H.B. Lima, D. Profeti, M. Chatenet, D. Riello, E.A. Ticianelli, E.R. Gonzalez, Electro-oxidation of ethanol on Rh/Pt and Ru/Rh/Pt sub-monolayers deposited on Au/C nanoparticles, Electrocatalysis 1 (2010) 72–82, doi:10.1007/s12678-010-0014-1.

[9] L.G.S. Pereira, V.A. Paganin, E.A. Ticianelli, Investigation of the CO tolerance mechanism at several Pt-based bimetallic anode electrocatalysts in a PEM fuel cell, Electrochim. Acta 54 (2009) 1992–1998, doi:10.1016/j.electacta.2008.07.003.

[10] W. Zhou, Z. Zhou, S. Song, W. Li, G. Sun, P. Tsiakaras, Q. Xin, Pt based anode catalysts for direct ethanol fuel cells, Appl. Catal. B Environ. 46 (2003) 273–285, doi:10.1016/S0926-3373(03)00218-2.

[11] L. Jiang, A. Hsu, D. Chu, R. Chen, Ethanol electro-oxidation on Pt / C and PtSn / C catalysts in alkaline and acid solutions, Int. J. Hydrog. Energy 35 (2010) 365–372, doi:10.1016/j.ijhydene.2009.10.058.

[12] D.R.M. Godoi, J. Perez, H.M. Villullas, Alloys and oxides on carbon-supported Pt-Sn electrocatalysts for ethanol oxidation, J. Power Sources 195 (2010) 3394–3401, doi:10.1016/j.jpowsour.2009.12.037.

[13] C. Lamy, C. Coutanceau, Electrocatalysis of Alcohol Oxidation Reactions at Platinum Group Metals, 2012. 10.1039/9781849734783-00001.

[14] J. Ribeiro, D.M. Dos Anjos, J.M. Léger, F. Hahn, P. Olivi, A.R. De Andrade, G. Tremiliosi-Filho, K.B. Kokoh, Effect of W on PtSn/C catalysts for ethanol electrooxidation, J. Appl. Electrochem. 38 (2008) 653–662, doi:10.1007/s10800-008-9484-8.

[15] P.E. Tsiakaras, PtM/C (M = Sn, Ru, Pd, W) based anode direct ethanol-PEMFCs: structural characteristics and cell performance, J. Power Sources 171 (2007) 107–112, doi:10.1016/j.jpowsour.2007.02.005.

[16] A.L.N. Pinheiro, A. Oliveira-Neto, E.C. De Souza, J. Perez, V.A. Paganin, E.A. Ticianelli, E.R. Gonzalez, Electrocatalysis on noble metal and noble metal alloys dispersed on high surface area carbon, J. New Mater. Electrochem. Syst. 6 (2003) 1–8.

[17] V.A. Paganin, E.A. Ticianelli, E.R. Gonzalez, Development and electrochemical studies of gas diffusion electrodes for polymer electrolyte fuel cells, J. Appl. Electrochem. 26 (1996) 297–304, doi:10.1007/BF00242099.

[18] K.C. Neyerlin, H.A. Gasteiger, C.K. Mittelsteadt, J. Jorne, W. Gu, Effect of relative humidity on oxygen reduction kinetics in a PEMFC, J. Electrochem. Soc. 152 (2005) A1073, doi:10.1149/1.1897368.

[19] P. Wnuk, R. Jurczakowski, A. Lewera, Electrochemical characterization of low-temperature direct ethanol fuel cells using direct and alternate current methods, Electrocatalysis 11 (2020) 121–132, doi:10.1007/s12678-019-00559-w.

[20] J.R.C. Salgado, E. Antolini, E.R. Gonzalez, Preparation of Pt-Co/C electrocatalysts by reduction with borohydride in acid and alkaline media: the effect on the performance of the catalyst, J. Power Sources 138 (2004) 56–60, doi:10.1016/j.jpowsour.2004.06.011.

[21] A. Hassan, V.A. Paganin, E.A. Ticianelli, Investigation of carbon supported PtW catalysts as CO tolerant anodes at high temperature in proton exchange membrane fuel cell, J. Power Sources 325 (2016) 375–382, doi:10.1016/j.jpowsour.2016.06.043.

[22] A. Hassan, A. Carreras, J. Trincavelli, E.A. Ticianelli, Effect of heat treatment on the activity and stability of carbon supported PtMo alloy electrocatalysts for hydrogen oxidation in proton exchange membrane fuel cells, J. Power Sources 247 (2014) 712–720, doi:10.1016/j.jpowsour.2013.08.138.

[23] E.I. Santiago, G.A. Camara, E.A. Ticianelli, CO tolerance on PtMo/C electrocatalysts prepared by the formic acid method, Electrochim. Acta 48 (2003) 3527–3534, doi:10.1016/S0013-4686(03)00474-2.

[24] A.F. Innocente, A.C.D. Ângelo, Electrocatalysis of oxidation of hydrogen on platinum ordered intermetallic phases: kinetic and mechanistic studies, J. Power Sources 162 (2006) 151–159, doi:10.1016/j.jpowsour.2006.06.057.

[25] E. Santos, L.M.C. Pinto, G. Soldano, A.F. Innocente, A.C.D. Ângelo, W. Schmickler, Hydrogen oxidation on ordered intermetallic phases of platinum and tin – A combined experimental and theoretical study, Catal. Today 202 (2013) 191–196, doi:10.1016/j.cattod.2012.07.044.

[26] R. Makharia, M.F. Mathias, D.R. Baker, Measurement of catalyst layer electrolyte resistance in PEFCs using electrochemical impedance spectroscopy, J. Electrochem. Soc. 152 (2005) A970, doi:10.1149/1.1888367.

[27] K.C. Neyerlin, W. Gu, J. Jorne, A. Clark, H.A. Gasteiger, Cathode catalyst utilization for the ORR in a PEMFC, J. Electrochem. Soc. 154 (2007) B279, doi:10.1149/1.2400626.

[28] A.A.K.M. Eikerling, Electrochemical impedance of the cathode catalyst layer in polymer electrolyte fuel cells, J. Electroanal. Chem. 475 (1999) 107–123, doi:10.1016/S0022-0728(99)00335-6.

[29] J.J. Giner-Sanz, E.M. Ortega, V. Pérez-Herranz, Montecarlo based quantitative Kramers-Kronig test for PEMFC impedance spectrum validation, Int. J. Hydrog. Energy 40 (2015) 11279–11293, doi:10.1016/j.ijhydene.2015.03.135.

[30] J. St-Pierre, PEMFC contamination model: foreign cation exchange with ionomer protons, J. Power Sources 196 (2011) 6274–6283, doi:10.1016/j.jpowsour.2011.04.008.

[31] T. Lopes, D.S. Kim, Y.S. Kim, F.H. Garzon, Ionic transport and water vapor uptake of ammonium exchanged perfluorosulfonic acid membranes, J. Electrochem. Soc. 159 (2012) B265–B269, doi:10.1149/2.040203jes.

[32] T. Lopes, J.-.M. Sansiñena, R. Mukundan, D.S. Hussey, D.L. Jacobson, F.H. Garzon, Diagnosing the effects of ammonia exposure on PEFC cathodes, J. Electrochem. Soc. 161 (2014) F703–F709, doi:10.1149/2.028406jes.

[33] I.M. Smallwood, Handbook of Organic Solvent Properties, Handb. Org. Solvent Prop. (2012) 1–306, doi:10.1016/C2009-0-23646-4.

[34] D. Mackay, W.-.Y. Shiu, W.-.Y. Shiu, S.C. Lee, Handbook of Physical-Chemical Properties and Environmental Fate for Organic Chemicals, 2006. 10.1201/9781420044393.

[35] K.I. Gursahani, R. Alcalá, R.D. Cortright, J.A. Dumesic, Reaction kinetics measurements and analysis of reaction pathways for conversions of acetic acid, ethanol, and ethyl acetate over silica-supported Pt, Appl. Catal. A Gen. 222 (2001) 369–392, doi:10.1016/S0926-860X(01)00844-4.

[36] F.L.S. Purgato, P. Olivi, J.M. Léger, A.R. de Andrade, G. Tremiliosi-Filho, E.R. Gonzalez, C. Lamy, K.B. Kokoh, Activity of platinum-tin catalysts prepared by the Pechini-Adams method for the electrooxidation of ethanol, J. Electroanal. Chem. 628 (2009) 81–89, doi:10.1016/j.jelechem.2009.01.010.

[37] A.F.F. De Lima, R.C. Colman, F.M.Z. Zotin, L.G. Appel, Acetaldehyde behavior over platinum based catalyst in hydrogen stream generated by ethanol reforming, Int. J. Hydrog. Energy. (2010), doi:10.1016/j.ijhydene.2010.09.030.

[38] I. Kutsche, G. Giidehaus, D. Schuler, A. Schumpe, Aqueous Alcohol Solutions, (1984) 286–287.

[39] R.B. Kutz, B. Braunschweig, P. Mukherjee, R.L. Behrens, D.D. Dlott, A. Wieckowski, Reaction pathways of ethanol electrooxidation on polycrystalline platinum catalysts in acidic electrolytes, J. Catal. 278 (2011) 181–188, doi:10.1016/j.jcat.2010.11.018.

[40] F. Vigier, C. Coutanceau, F. Hahn, E.M. Belgsir, C. Lamy, On the mechanism of ethanol electro-oxidation on Pt and PtSn catalysts: electrochemical and in situ IR reflectance spectroscopy studies, J. Electroanal. Chem. 563 (2004) 81–89, doi:10.1016/j.jelechem.2003.08.019.

[41] M.Z.F.Z.F. Kamarudin, S.K.K. Kamarudin, M.S.S. Masdar, W.R.W.R.W. Daud, Review: direct ethanol fuel cells, Int. J. Hydrog. Energy. 38 (2013) 9438–9453, doi:10.1016/j.ijhydene.2012.07.059.

[42] J.C.M. Silva, L.S. Parreira, R.F.B. De Souza, M.L. Calegaro, E.V. Spinacé, A.O. Neto, M.C. Santos, PtSn/C alloyed and non-alloyed materials: differences in the ethanol electro-oxidation reaction pathways, Appl. Catal. B Environ. 110 (2011) 141–147, doi:10.1016/j.apcatb.2011.08.036.